Journal of Power Sources 196 (2011) 962–967

Contents lists available at ScienceDirect

Journal of Power Sources

journal homepage: www.elsevier.com/locate/jpowsour

Micro-tubular solid oxide fuel cells with graded anodes fabricated with a phase inversion method

Ling Zhao [a], Xiaozhen Zhang [a,b], Beibei He [a], Beibei Liu [a], Changrong Xia [a,*]

[a] CAS Key Laboratory of Materials for Energy Conversion, Department of Materials Science and Engineering, University of Science and Technology of China, Hefei, Anhui 230026, China

[b] Key Laboratory of Jiangxi Universities for Inorganic Membranes, School of Material Science and Engineering, Jingdezhen Ceramic Institute, Jingdezhen 333001, China

ARTICLE INFO

Article history:
Received 2 July 2010
Received in revised form 26 August 2010
Accepted 26 August 2010
Available online 27 September 2010

Keywords:
Micro-tubular solid oxide fuel cells
Graded anode
Phase inversion
Proton conductor

ABSTRACT

Micro-tubular proton-conducting solid oxide fuel cells (SOFCs) are developed with thin film $BaZr_{0.1}Ce_{0.7}Y_{0.1}Yb_{0.1}O_{3-\delta}$ (BZCYYb) electrolytes supported on Ni-BZCYYb anodes. The substrates, NiO-BZCYYb hollow fibers, are prepared by an immersion induced phase inversion technique. The resulted fibers have a special asymmetrical structure consisting of a sponge-like layer and a finger-like porous layer, which is propitious to serving as the anode supports for micro-tubular SOFCs. The fibers are characterized in terms of porosity, mechanical strength, and electrical conductivity regarding their sintering temperatures. To make a single cell, a dense BZCYYb electrolyte membrane about 20 μm thick is deposited on the hollow fiber by a suspension-coating process and a porous $Sm_{0.5}Sr_{0.5}CoO_3$ (SSC)-BZCYYb cathode is subsequently fabricated by a slurry coating technique. The micro-tubular proton-conducting SOFC generates a peak power density of 254 mW cm^{-2} at 650 °C when humidified hydrogen is used as the fuel and ambient air as the oxidant.

© 2010 Elsevier B.V. All rights reserved.

1. Introduction

In recent years, solid oxide fuel cells (SOFCs) have received tremendous attention due to their high energy conversion efficiency, low emissions and excellent fuel flexibility [1–3]. These cells are often designed to have either a planar or a tubular geometric configuration. The tubular type is relatively mature in terms of designing and manufacturing technology, has attracted much interest because it has better thermo-cycling behavior, and is easier to seal, compared with the planar type [4–6]. Moreover, it is interesting to note that several potential benefits appear when the diameter gets smaller, on the micron scale, such as higher volumetric power density and higher thermal shock resistance [7], which is a distinct advantage in applications where start-up time is critical.

Micro-tubular SOFCs are categorized as anode-supported, electrolyte-supported and cathode-supported structures, depending on the component providing the mechanical strength to the micro-tubular cells. Anode-supported cells are favored for three main reasons: they allow for the fabrication of a very thin layer of electrolyte, there is no need to use any sophisticated technique of depositing the electrode inside the micro-tubes and lastly, they facilitate designing current collectors [8]. These characters have promoted the research for anode-supported cells. Generally, the anode substrate is fabricated by traditional extrusion techniques [9–11]. However, the as-prepared tubes have a poor microstructure which gives rise to a large interfacial polarization resistance. Recently, an immersion induced phase inversion technique [12–14] has been introduced to fabricate ceramic hollow fiber membranes with thin walls and an asymmetric structure that greatly improves the microstructures as the anode substrates. More importantly, this method does not require expensive equipments and its operation is also relatively simple [14]. Therefore, cost reduction can also be expected for micro-tubular SOFCs.

Up to now, the research of micro-tubular SOFCs is focused on oxygen ion-conducting electrolytes, while little attention is paid to proton-conducting electrolytes. Anode-supported micro-tubular proton-conducting SOFCs have some interesting features compared with oxygen ion-conducting ones. Firstly, forming water vapor at the cathode side helps to improve the EMF and the fuel utilization efficiency of SOFC system [15,16]. Secondly, water vapor at the cathode side (outside of the tubular) is easier to diffuse away than that at the anode side (inside of the tubular) since the inner diameter is much smaller than the outer.

In this work, a phase inversion method is used to fabricate graded anode substrates for micro-tubular proton-conducting SOFCs based on $BaZr_{0.1}Ce_{0.7}Y_{0.1}Yb_{0.1}O_{3-\delta}$ (BZCYYb) electrolytes, which are proton conductors that display both satisfying conductivity and sufficient chemical stability over a wide range of conditions relevant to fuel cell operation.

* Corresponding author. Tel.: +86 551 3607475; fax: +86 551 3601592.
E-mail address: xiacr@ustc.edu.cn (C. Xia).

0378-7753/$ – see front matter © 2010 Elsevier B.V. All rights reserved.
doi:10.1016/j.jpowsour.2010.08.074

2. Experimental

2.1. Powders preparation

The micro-tubular cells consist of Ni-BZCYYb ($BaZr_{0.1}Ce_{0.7}Y_{0.1}Yb_{0.1}O_{3-\delta}$) composite anodes, BZCYYb electrolytes, and SSC ($Sm_{0.5}Sr_{0.5}CoO_3$)-BZCYYb composite cathodes. NiO powder is from Jinchuan Group (China), while BZCYYb and SSC powders were synthetized via a combustion process [17] with citric acid and using nitrates as the precursors. $Ba(NO_3)_2$, $Zr(NO_3)_4$, $Ce(NO_3)_3$, $Y(NO_3)_3$ and $Yb(NO_3)_3$ were dissolved in distilled water at the stoichiometric ratio for the nominal composition of $BaZr_{0.1}Ce_{0.7}Y_{0.1}Yb_{0.1}O_{3-\delta}$ to form a BZCYYb stock solution. Citric acid was then added, which was used as complexation agent. And citric acid/metal molar ratio was set at 1.5. The solution was then heated on a hot-plate till self-combustion occurred. The as-synthesized powder was subsequently calcined at 1000 °C for 3 h to obtain the BZCYYb powders, which exhibited a perovskite phase structure. $Sm_{0.5}Sr_{0.5}CoO_3$ (SSC) powders were synthesized with the same process, while calcined at 950 °C for 3 h to form the provskite phase.

2.2. Fabrication of micro-tubular solid oxide fuel cells with graded anodes

NiO and BZCYYb powders with a weight ratio of 60:40 were mixed as the starting materials for anode supports. *N*-Methyl-2-pyrrolidone (NMP, Chemical Pure, Sinopharm Chemical Reagent Co., Ltd, China), polyethersulfone (PESf, Radel A-100, Solvay Advanced Polymers, L.L.C.) and polyvinylpyrrolidone (PVP, K30, Chemical Pure, Sinopharm Chemical Reagent Co., Ltd, China) were used as the solvent, binder and dispersant, respectively. PESf and PVP were dissolved in a NMP solvent to prepare the spinning suspension, to which the mixed NiO and BZCYYb powder was added. The suspension was stirred for at least 24 h to ensure that the ceramic powder was well dispersed in the polymer solution. The as-prepared suspension was then transferred to a gas-tight spinning reservoir and degassed for 0.5 h at room temperature. Immediately after degassing, the spinning suspension was pressurized at 0.5 bar using nitrogen and was subsequently extruded through a tube-in-orifice spinneret with orifice diameter and inner diameter of 2.5 and 1.0 mm, respectively. The fibers emerging from the spinneret passed through an air gap of 15 cm and immersed in the external coagulant for complete gelation. Suspension compositions and related spinning parameters are given in Table 1. The hollow fibers were then retained in a water bath for 24 h to allow of complete solidification and then pre-sintered at 1300, 1350 and 1400 °C for 5 h to form different anode substrates.

The BZCYYb electrolyte was deposited on the outside surface of the fiber using a suspension-coating technique. BZCYYb powder was dispersed in ethanol solvent and ball-milled for 24 h to form a suspension with 10 wt.% BZCYYb. The hollow fiber anode substrates were then dipped to the suspension. After drawing and drying, a green bi-layer was formed consisting of the NiO-BZCYYb substrate and BZCYYb electrolyte. The bi-layer structure was co-fired at 1300, 1350 and 1400 °C for 5 h to densify the electrolyte. Composite BZCYYb-SSC electrodes were then fabricated by a screen printing method [18] and fired at 950 °C for 3 h in air.

Table 1
Spinning conditions for NiO-BZCYYb hollow fibers.

Parameters	Values
Compositions of spinning solution	
NiO	36.0%
BZCYYb	24.0%
PESf	6.4%
NMP	32.0%
PVP	1.6%
Spinneret dimension: ID/OD	1.0 mm/2.5 mm
Internal/external coagulant	Deionized water/deionized water
Spinning temperature	20 °C
Relative humidity	40%
Flow rate of internal coagulant	30 mL min^{-1}
Air gap	15.0 cm
Nitrogen pressure	0.5 bar

2.3. Characterization

The phase structures of the as-synthesized powders were inspected by X-ray diffraction (PW-1730). The microstructure of the hollow fiber was observed with scanning electron microscopy (SEM) (JEOL, JSM-6700F). The relative density of hollow fibers was determined by Archimedes' method. Electrical conductivity was investigated using the standard DC four-probe technique with H.P. multimeter (Model 34401). The bending strength of hollow fibers was determined by the three-point bending method using a universal testing machine (Instron 5566), with a crosshead speed of 0.25 mm min^{-1} and a span length of 30 mm.

Single cells were tested at 600 and 650 °C using a home-developed-cell-testing system with humidified hydrogen (~3% H_2O) as the fuel and ambient air as the oxidant, respectively. The flow rate of the fuel was about 60 ml min^{-1}. An Electrochemical Workstation (IM6e, Zahner) was used to characterize the electrochemical performance. The current–voltage curve was obtained using a galvanostat mode and the electrochemical impedance spectra were measured at open-circuit conditions in the frequency range from 0.1 Hz to 1 MHz (10 mV as AC amplitude).

3. Results and discussion

3.1. Compatibility of cell components

Fig. 1 is the XRD patterns of the cell components. A pure phase of perovskite structured SSC is formed when the resulted ash is sintered at 950 °C for 3 h (Fig. 1a), which agrees well with the previous reported phase structure of SSC [19]. Fig. 1b shows that the phase structure of electrolyte powder ($BaZr_{0.1}Ce_{0.7}Y_{0.1}Yb_{0.1}O_{3-\delta}$) sintered at 1350 °C for 5 h exhibits a perovskite phase structure, which is identical to those of the barium cerate standard (JCPDS Card No. 82-2425), implying the electrolyte membrane is the pure

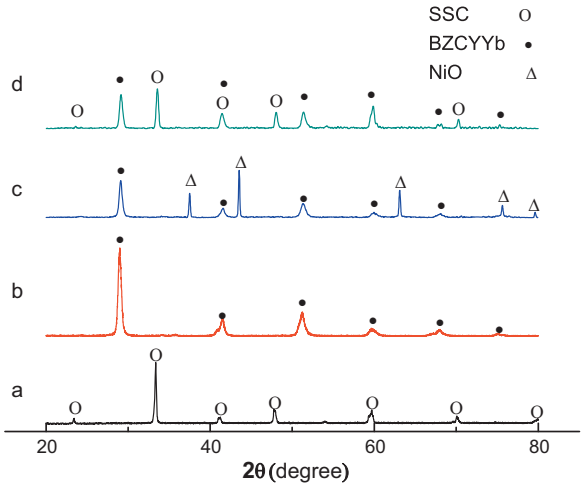

Fig. 1. XRD diffraction patterns of (a) a $Sm_{0.5}Sr_{0.5}CoO_3$ (SSC) powder fired at 950 °C, (b) a $BaZr_{0.1}Ce_{0.7}Y_{0.1}Yb_{0.1}O_{3-\delta}$ (BZCYYb) powder fired at 1350 °C, (c) a NiO-BZCYYb anode substrate co-fired at 1350 °C, and (d) a SSC-BZCYYb cathode powder co-fired at 950 °C.

perovskite phase of BZCYYb. It can be seen that there are only peaks corresponding to either NiO or BZCYYb when the anode substrate is sintered at 1350 °C for 5 h (Fig. 1c), suggesting BZCYYb is chemically compatible with NiO under cell fabrication conditions. When SSC-BZCYYb composite is sintered at 950 °C for 3 h (Fig. 1d), no obvious reactions occur between SSC and BZCYYb. The results are consistent with Yang et al. [20], who found that there are no observable chemical reactions between SSC and BZCY ($BaZr_{0.1}Ce_{0.7}Y_{0.2}O_{3-\delta}$) when they are co-fired below 1000 °C.

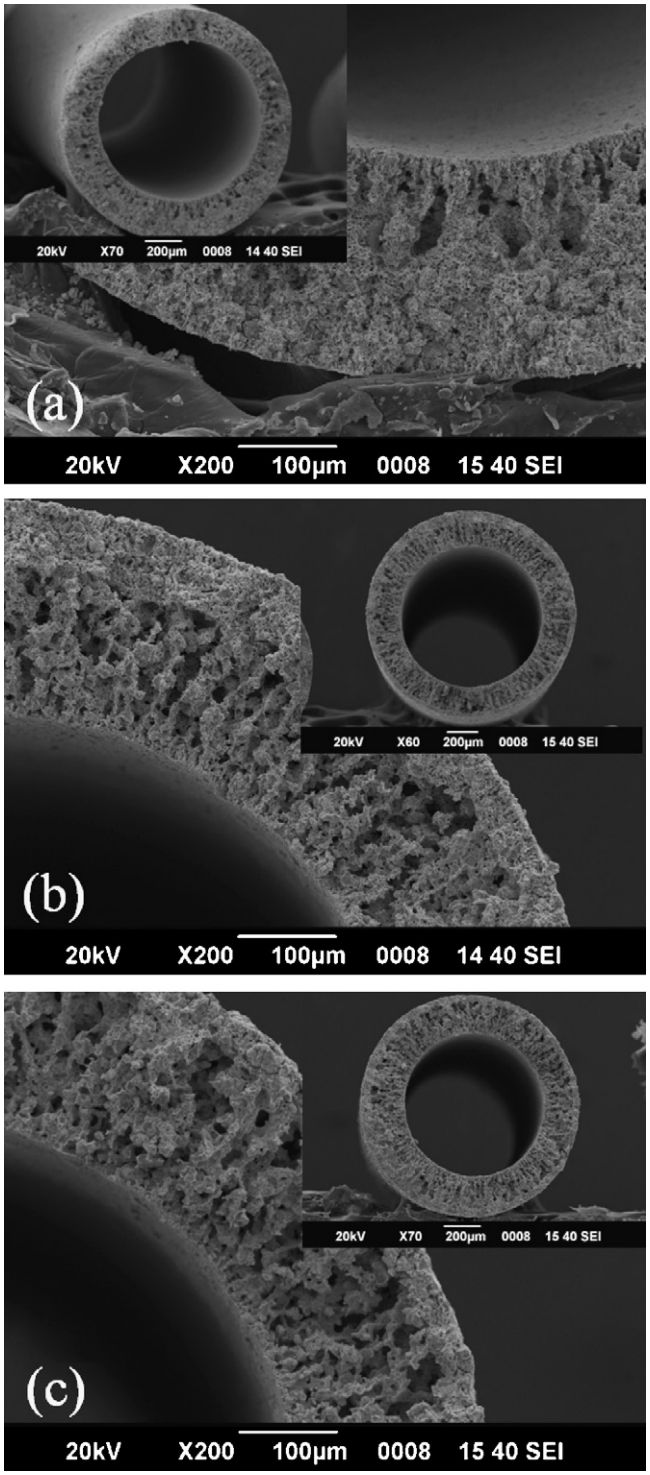

Fig. 2. Fractured surface microviews of NiO-BZCYYb hollow fibers sintered for 5 h at (a) 1300 °C, (b) 1350 °C, and (c) 1400 °C.

3.2. Characteristics of hollow fiber substrates

Fig. 2 shows the cross-sectional micrographs of NiO-BZCYYb hollow fibers sintered at 1300, 1350, and 1400 °C for 5 h. The cross-sectional structures of the NiO-BZCYYb hollow fibers exhibit a sponge-like porous layer on the outer side integrated with a finger-like porous layer on the inner side. The microstructure is very similar to that reported for micro-tubular SOFCs based on oxygen ion-conducting electrolytes [14]. The inside finger-like porous layer may greatly accelerate mass transfer of the fuel [21], while the outside sponge-like porous layer could provide much TPBs [14]. The formation of such asymmetric structure may be attributed to the different precipitation rates within the hollow fibers occurring during the spinning process. The rapid precipitation occurred on the outer side due to the contact with large quantities of external coagulant resulting in the formation of microporous structure while the slow precipitation on the inner side gives rise to the macro voids or the finger-like pores [22,23].

As anode substrates, the hollow fibers should provide enough pores to transport the fuel. Fig. 3 shows the porosity of NiO-BZCYYb and Ni-BZCYYb hollow fibers which are sintered at different temperatures. Increasing the sintering temperature from 1300 to 1400 °C, the NiO-BZCYYb porosity decreases gradually from 44.5 to 32.8%, and after reduction, the porosity decreases from 60.7 to 50.8%. The porosity measurement is consistent with the microfeatures shown in Fig. 2. The porosity of Ni-BZCYYb hollow fibers estimated from the total reduction of NiO in NiO-BZCYYb is also plotted in the Fig. 3 for comparison. It can be seen that the predicted and measured values are in good agreement. As compared to NiO-YSZ fibers fabricated by the same phase inversion process reported by Yang et al. and Droushiotis et al. [14,24], the porosity of NiO-BZCYYb is slightly higher than that reported by Yang et al, while lower than that reported by Droushiotis et al. The result may be attributed to the different solid content of the starting suspension, a high content usually results in low porosity. According to percolation theory, the porosity of anode active reaction field, which is about 10 μm, should be controlled between 30% and 40% [25]. Therefore, the average porosity of the Ni-BZCYYb fiber must be much higher so that the active sponge-like porous layer could have 30–40% porosity since the finger-like layer is more porous.

The mechanical strength of fuel cell elements is critically important for a number of reasons [26]. The elements must be able to be handled without breakage during fabrication and stack assembly, and must also survive during the thermal cycling which occurs dur-

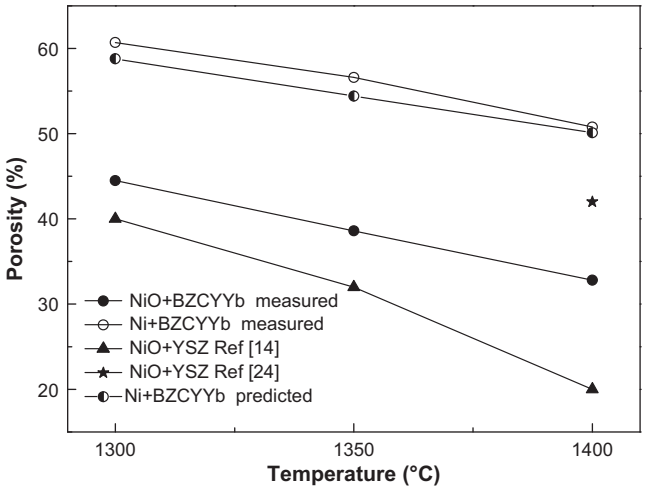

Fig. 3. Porosity of the Ni-BZCYYb and NiO-BZCYYb hollow fibers as a function of sintering temperature.

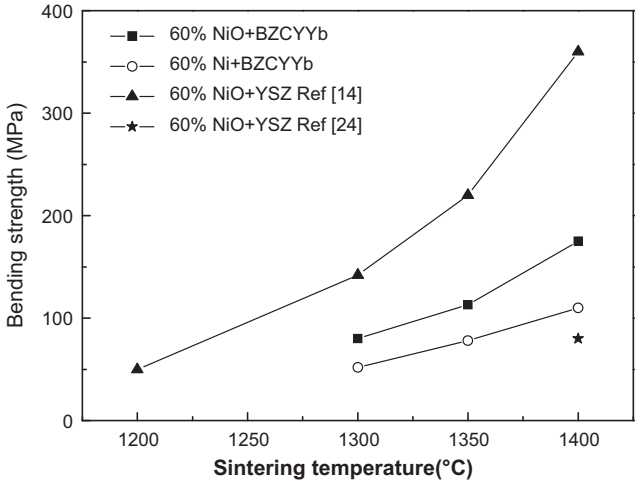

Fig. 4. Bending strength of the hollow fibers as a function of sintering temperature.

ing normal operation. The bending strength of the hollow fibers is determined by the three-point bending method according the equation as follows [27]:

$$\sigma F = \frac{8FLD}{\pi(D^4 - d^4)}$$

where F is the measured force at which the fracture occurred and L, D, and d are the length, the outer diameter, and the inner diameter of the hollow fibers, respectively. The results are shown in Fig. 4.

The bending strength increases with the increase of sintering temperature, which can be attributed to the stronger bonding created between the cermet particles at higher sintering temperatures. For NiO-BZCYYb sintered at 1300 °C for 5 h, the bending strength is about 80 MPa, while a much high strength of 175 MPa can be obtained when the sintering temperature is increased to 1400 °C. Actually, the fibers sintered at 1400 °C show sufficient mechanical strength to serve as anodes for anode-supported SOFCs [27]. The bending strength of Ni-BZCYYb, which is formed by reducing NiO-BZCYYb, is also shown in Fig. 4. The strength is significantly decreased after NiO is reduced. Such decrease is resulted from the reduction process, which not only weakens the bonding of the cermet particles but also increases the porosity. The bending strength of NiO-BZCYYb is slightly higher than that of NiO-YSZ as reported by Droushiotis et al. [24], while lower than that by Yang et al. [14]. The difference in strength may be attributed to the different anode composition and microstructure.

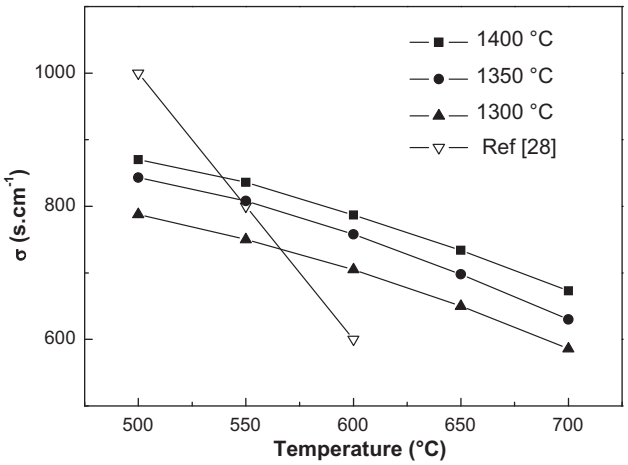

Fig. 5. Temperature dependence of conductivity for Ni-BZCYYb hollow fibers.

Electrical conductivity is another important parameter for the hollow fibers in their role as the anode supports, because the Ni-BZCYYb fibers not only provide the sites for electrochemical reactions, but also serve as current collectors. Fig. 5 shows the electrical conductivity of Ni-BZCYYb hollow fibers derived at different temperatures. The overall electrical conductivity is actually given by the Ni particles since the conductivity of BZCYYb is negligible compared to Ni. The conductivity decreases with the temperature as expected [28]. As the sintering temperature increases, the porosity is reduced, resulting in enhanced conductivity as shown in Fig. 5.

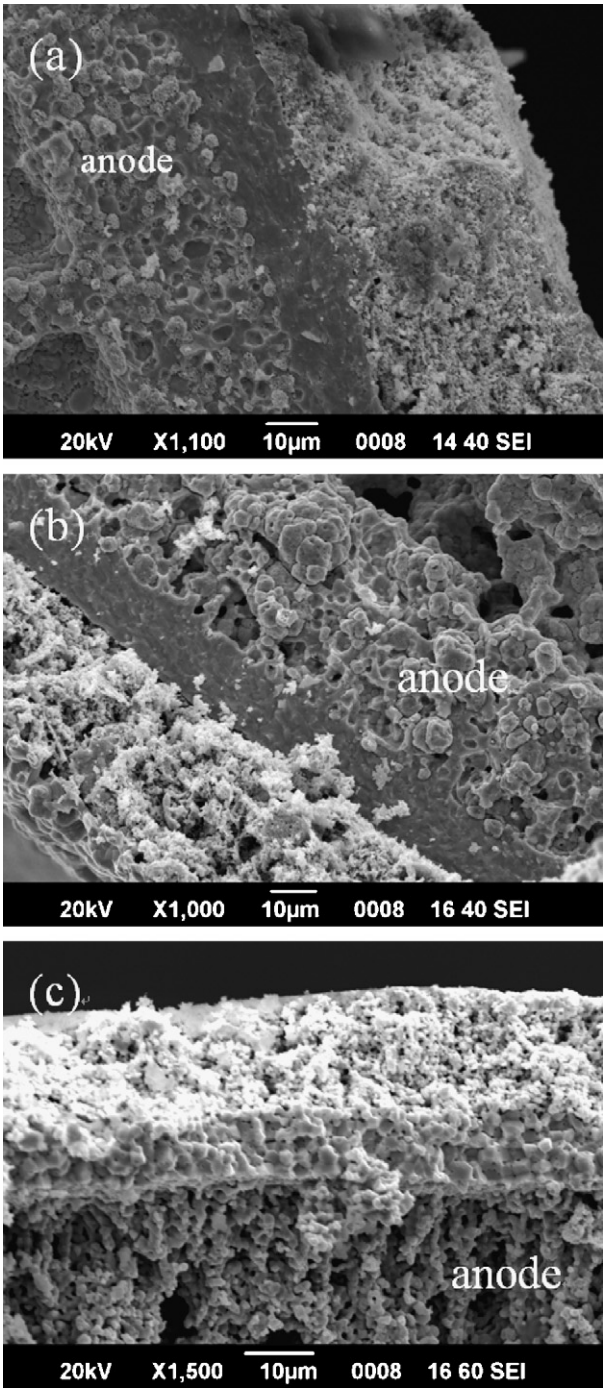

Fig. 6. Cross-sectional views of single cells with anode–electrolyte bi-layers sintered at: (a) 1400 °C, (b) 1350 °C, and (c) 1300 °C.

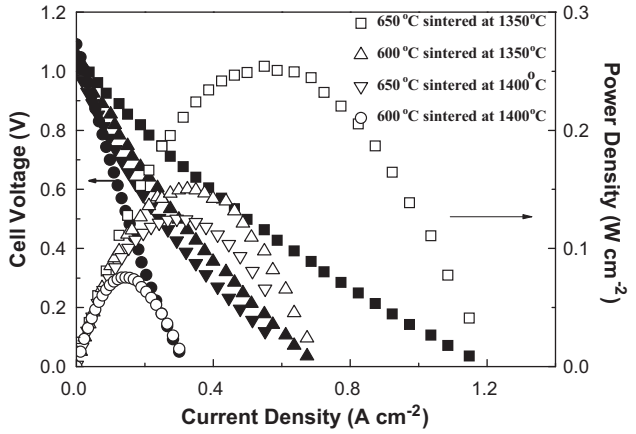

Fig. 7. Typical current–voltage characteristics and the corresponding power densities as a function of current densities for fuel cells with a configuration of Ni-BZCYYb/BZCYYb/SSC-BZCYYb.

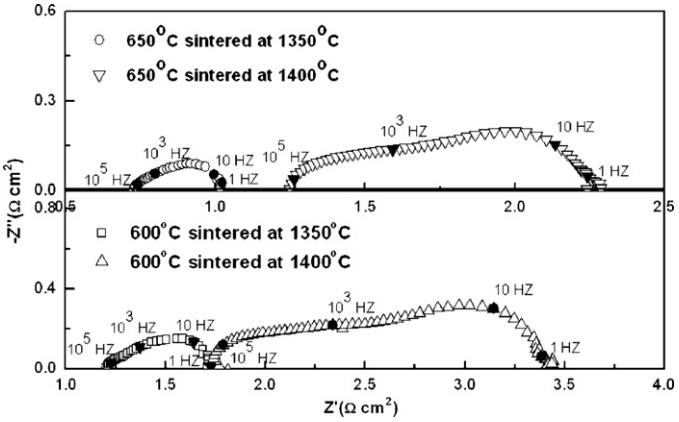

Fig. 8. Impedance spectra of single cells measured under open-circuit condition at 650 and 600 °C.

3.3. Single cell performance

To make single cells, the electrolyte powders are deposited on un-sintered NiO-BZCYYb hollow fibers, and then co-fired at 1300, 1350, and 1400 °C for 5 h. Fig. 6 shows the SEM pictures of the fractured surfaces. When it is sintered at 1400 °C, a relatively dense microstructure of sponge-like layer is observed next to the dense electrolyte. The dense layer is supposed to be the active anode. But its relatively low porosity might limit gas diffusion and thus cause high electrode polarization resistance. When it is sintered at 1300 °C, however, the electrolyte layer is not sense enough. When it is sintered at 1350 °C, the microstructure of the cell with about 20 μm dense electrolyte and 40 μm porous anode active layer might show high fuel cell performance.

A mixed proton, oxide ion and electron conducting cathode extends the TPB from the interface to the entire cathode, thereby greatly accelerating the charge transfer reaction [29]. Therefore, a fuel cell based on proton-conducting electrolyte using a mixed conducting cathode will be able to reduce the resistance for oxygen reduction reactions. In this work, single cells with SSC-BZCYYb composite cathodes are characterized at 600 and 650 °C. Fig. 7 shows the *I–V* and *I–P* curves of the single cells prepared with different sintering temperatures and measured with humidified hydrogen (about 3% H_2O) as the fuel and ambient as the oxidant. The results for the cell sintered at 1300 °C are not shown here since the OCV is very low due to the porous electrolyte (as shown in Fig. 6c). Peak power densities of 254 and 150 mW cm^{-2} are obtained at 650 and 600 °C respectively for the cell sintered at 1350 °C. The power density decreases when the cell is sintered at 1400 °C although the OCV is high enough, which might due to the relatively dense anode active layer. It should be noted that the micro-tubular cells exhibit lower power density than the values of planar cells, which can be as high as 660 mW cm^{-2} at 650 °C for a cell with 10 μm electrolyte [30].

Fig. 8 shows the AC impedance spectroscopy measured under open-circuit conditions. The high frequency intercept at the real axis corresponds to the ohmic resistance of the cell (Ro), including ionic resistance of the electrolyte, electronic resistance of the electrodes, and contact resistance associated with interfaces between the leading wires and the electrodes, while the low frequency intercept corresponds to the total cell resistance (Rtotal). Therefore, the difference between the high frequency and low frequency intercepts with the real axis represents the total interfacial polarization resistance (*R*p), including the cathode–electrolyte interface resistance and the anode–electrolyte interface resistance [31]. As expected, the cell with electrolyte fired at 1350 °C shows the lower interfacial polarization resistances. It is possible that the sponge-like porous layer which is relatively dense causes high anodic polarization resistance. As for the cell fired at 1350 °C, increasing the measuring temperature results in a significant reduction of the interfacial polarization resistances, from 0.51 Ω cm^2 at 600 °C to 0.28 Ω cm^2 at 650 °C. The ohmic resistance is 0.73 Ω cm^2 at 650 °C. The proton conductivity of BZCYYb is 0.03 S cm^{-1} at 650 °C [30], so the ionic resistance of a 20-μm-thick BZCYYb electrolyte is about 0.067 Ω cm^2, which is about 9% of the ohmic resistance. Therefore, the ohmic resistance of the micro-tubular fuel cell is dominated by the resistance associated with the electrodes and current collectors. A similar behavior has been reported by Suzuki et al. [32] for micro-tubular fuel cells with Ni-YSZ anodes. Presently, current collection remains a challenge for micro-tubular solid oxide fuel cells.

4. Conclusions

Hollow fiber NiO-BZCYYb substrates have been successfully fabricated by the phase inversion method. The fibers possess an asymmetric structure comprising of a microporous layer integrated with a finger-like porous structure. Such structure is excellent as the anode support for solid oxide fuel cells with proton conductors. The fiber's mechanical strength and electrical conductivity increase while its porosity decreases with sintering temperature. This makes an optimized sintering temperature of 1350 °C for the anode–electrolyte bi-layers. A micro-tubular proton-conducting single cell consisting of a Ni-BZCYYb anode, a BZCYYb electrolyte, and a SSC-BZCYYb cathode generates a peak power density of 254 mW cm^{-2} at 650 °C. However, current collection remains a challenge for micro-tubular solid oxide fuel cells for practical applications.

Acknowledgments

This work was supported by the Natural Science Foundation of China (10979046 and 50730002) and the Ministry of Science and Technology of China (2007AA05Z151).

References

[1] B.C.H. Steele, A. Heinzel, Nature 414 (2001) 345.
[2] Y.H. Huang, R.I. Dass, Z.L. Xing, J.B. Goodenough, Science 312 (2006) 254.
[3] Z.L. Zhan, S.A. Barnett, Science 308 (2005) 844.
[4] N.M. Sammes, Y. Du, R. Bove, J. Power Sources 145 (2005) 428.
[5] A.V. Akkaya, Int. J. Energy Res. 31 (2007) 79.
[6] J.X. Jia, R.Q. Jiang, S.Q. Shen, A. Abudula, Environ. Energy Eng. 54 (2008) 554.

[7] S.C. Singhal, K. Kendall, High Temperature Solid Oxide Fuel Cells: Fundamentals, Design and Applications, Elsevier, New York, 2003, p. 219.
[8] N. Droushiotis, U. Doraswami, K. Kanawka, G.H. Kelsall, K. Li, Solid State Ionics 180 (2009) 1091.
[9] Y. Funahashi, T. Shimamori, T. Suzuki, Y. Fujishiro, M. Awano, J. Power Sources 163 (2007) 731.
[10] T. Suzuki, Y. Funahashi, T. Yamaguchi, Y. Fujishiro, M. Awano, J. Alloys Compd. 451 (2008) 632.
[11] C.L. Yang, W. Li, S.Q. Zhang, L. Bi, R.R. Peng, C.S. Chen, W. Liu, J. Power Sources 187 (2009) 90.
[12] C.C. Wei, Q.Y. Chen, Y. Liu, K. Li, J. Membr. Sci. 320 (2008) 191.
[13] C. Jin, J. Liu, L.H. Li, Y.H. Bai, J. Membr. Sci. 341 (2009) 233.
[14] N.T. Yang, X.Y. Tan, Z.F. Ma, J. Power Sources 183 (2008) 14.
[15] K.D. Kreuer, Annu. Rev. Mater. Res. 33 (2003) 333.
[16] D. Hirabayashi, A. Tomita, S. Teranishi, T. Hibino, M. Sano, Solid State Ionics 176 (2005) 881.
[17] L. Zhao, B.B. He, B. Lin, H.P. Ding, S.L. Wang, Y.H. Ling, R.R. Peng, G.Y. Meng, X.Q. Liu, J. Power Sources 194 (2009) 835.
[18] L. Zhao, B.B. He, Q. Nian, Z.Q. Xun, R.R. Peng, G.Y. Meng, X.Q. Liu, J. Power Sources 194 (2009) 291.
[19] C.R. Xia, W. Rauch, F.L. Chen, M.L. Liu, Solid State Ionics 149 (2002) 11.
[20] L. Yang, C.D. Zuo, S.Z. Wang, Z. Cheng, M.L. Liu, Adv. Mater. 20 (2008) 3280.
[21] X.Y. Tan, Z.B. Pang, Z.S.M. Liu, J. Membr. Sci. 302 (2007) 109.
[22] J.F. Blanco, J. Sublet, Q.T. Nguyena, P. Schaetzel, J. Membr. Sci. 283 (2006) 27.
[23] S. Mok, D.J. Worsfold, A.E. Fouda, T. Matsuura, S. Wang, K. Chan, J. Membr. Sci. 100 (1995) 183.
[24] N. Droushiotis, U. Doraswanmi, K. Kanawka, G. Kelsall, K. Li, Solid State Ionics 180 (2000) 1091.
[25] M. Brown, S. Primdahl, M. Mogensen, J. Electrochem. Soc. 147 (2000) 475.
[26] B.R. Roy, N.M. Sammes, T. Suzuki, Y. Funahashi, M. Awano, J. Power Sources 188 (2009) 220.
[27] X.Z. Zhang, B. Lin, Y.H. Ling, Y.C. Dong, D.R. Fang, G.Y. Meng, X.Q. Liu, J. Alloys Compd. 494 (2010) 366.
[28] T. Suzuki, Y. Funahashi, T. Yamaguchi, Y. Fujishiro, M. Awano, Solid State Ionics 180 (2008) 546.
[29] L. Yang, Z. Liu, S.Z. Wang, Y.M. Choi, C.D. Zuo, M.L. Liu, J. Power Sources 195 (2010) 471.
[30] L. Yang, S.Z. Wang, K. Blinn, M.F. Liu, Z. Liu, Z. Cheng, M.L. Liu, Science 326 (2009) 126.
[31] L. Zhang, S.P. Jiang, W. Wang, Y.J. Zhang, J. Power Sources 170 (2007) 55.
[32] T. Suzuki, Z. Hasan, Y. Funahashi, T. Yamaguchi, Y. Fujishiro, M. Awano, Science 325 (2009) 852.